Available online at www.sciencedirect.com
SCIENCE DIRECT®
Journal of Solid State Chemistry 177 (2004) 4286–4292
JOURNAL OF SOLID STATE CHEMISTRY
www.elsevier.com/locate/jssc

Effect of capping and particle size on Raman laser-induced degradation of γ-Fe_2O_3 nanoparticles

K.S.K. Varadwaj[a], M.K. Panigrahi[b], J. Ghose[a,*]

[a]*Department of Chemistry, Indian Institute of Technology, Kharagpur, West Bengal-721302, India*
[b]*Department of Geology and Geophysics, Indian Institute of Technology, Kharagpur 721302, India*

Received 21 June 2004; received in revised form 16 August 2004; accepted 19 August 2004

Abstract

Diol capped γ-Fe_2O_3 nanoparticles are prepared from ferric nitrate by refluxing in 1,4-butanediol (9.5 nm) and 1,5-pentanediol (15 nm) and uncapped particles are prepared by refluxing in 1,2-propanediol followed by sintering the alkoxide formed. X-ray diffraction (XRD) shows that all the samples have the spinel phase. Raman spectroscopy shows that the samples prepared in 1,4-butanediol and 1,5-pentanediol and 1,2-propanediol (sintered at 573 and 673 K) are γ-Fe_2O_3 and the 773 K-sintered sample is Fe_3O_4. Raman laser studies carried out at various laser powers show that all the samples undergo laser-induced degradation to α-Fe_2O_3 at higher laser power. The capped samples are however, found more stable to degradation than the uncapped samples. The stability of γ-Fe_2O_3 sample with large particle size (15.4 nm) is more than the sample with small particle size (10.2 nm). Fe_3O_4 having a particle size of 48 nm is however less stable than the smaller γ-Fe_2O_3 nanoparticles.

Keywords: γ-Fe_2O_3; Nanoparticles; Capping; Raman laser degradation

1. Introduction

In the last decade, studies on nanocrystalline materials have attracted a lot of attention. This is mainly due to their unusual properties which have found wide applications in magnetic nanodevices, biomedical research, catalysis, etc. [1–3]. Among the various magnetic nanomaterials, γ-Fe_2O_3 is used in magnetic memory devices, color imaging, magnetic refrigeration, ferrofluids, catalysis and sensors [4–7]. Coating or capping the nanoparticles with polymers or organic moieties further enhances their applicability as it prevents agglomeration and the material becomes dispersible in aqueous or organic solvents [8]. The stable aqueous ferrofluids have many biomedical applications, e.g. in cell separation, as contrast agents in magnetic resonance imaging and in drug delivery [9,10].

Raman spectroscopy is an important experimental technique for studying the vibrational and structural properties of materials. In the study of ferrofluids Raman spectroscopy is used to probe the chemical species chemisorbed on the nanoparticle surface [11,12]. But in micro-Raman experiments the high power density of laser beam focused on a small spot size with diameter of few micrometers increases the local spot temperature to hundreds of degrees. This causes thermal transformation, oxidation, phase transition or decomposition of the sample [13]. The laser-induced thermal transformation was found to depend on the morphology of the sample. Although, considerable amount of work has been done on the Raman laser-induced phase transition studies particularly for some iron oxides, Raman laser studies on the nanocystalline solids have not yet been reported. In the present work, γ-Fe_2O_3 nanoparticles capped with a polyol has been synthesized by a one step method and its stability towards degradation has been studied with Raman laser. Effect of particle size on the stability of the γ-Fe_2O_3 nanoparticles has also been studied.

*Corresponding author. Fax: +91-3222-255303.
E-mail address: jayg@chem.iitkgp.ernet.in (J. Ghose).

0022-4596/$ - see front matter © 2004 Elsevier Inc. All rights reserved.
doi:10.1016/j.jssc.2004.08.025

2. Experimental

2.1. Sample preparation in 1,4-butanediol and 1,5-pentanediol

Surface-coated nanocrystalline γ-Fe_2O_3 was prepared by dissolving 4.04 g of ferric nitrate ($Fe(NO_3)_3 \cdot 9H_2O$, Merck) in 5 mL of diol. The reaction was initiated at 373 K by addition of the prepared solution to a two-necked round-bottom flask containing 20 mL of diol. As the temperature was slowly raised to 403 K, brown nitrous fumes evolved and the solution was allowed to stand at this temperature for 1 h. On complete removal of nitrous fumes, the solution was slowly heated to reflux. The color of the solution gradually changed to deep brown. After refluxing for 1 h the solution was cooled to room temperature and on addition of 30 mL of toluene–methanol mixture (1:1 v/v) a dark brown precipitate appeared which was then collected by centrifugation.

2.2. Sample preparation in 1,2-propanediol

Uncoated nanocrystalline γ-Fe_2O_3 was prepared by dissolving 4.04 g of ferric nitrate ($Fe(NO_3)_3 \cdot 9H_2O$, Merck) in 25 mL of 1,2-propanediol and heating the solution to 403 K for 1 h, when nitrous fume evolved and a dark yellow layered alkoxide precipitate was formed. On heating the alkoxide at 573 K, in Argon atmosphere, nanocrystalline γ-Fe_2O_3 was formed. The alkoxide was also heated to 673 and 773 K to obtain γ-Fe_2O_3 of varying particle size.

2.3. Characterization

X-ray diffraction (XRD) analyses of the oxide samples and intermediates were carried out with a Phillips X-ray diffraction unit (model PM 1710) using Ni-filtered CoK_α ($\lambda = 1.79$ Å) radiation. The crystallite size of the nanocrystalline samples were determined by X-ray line broadening analyses, applying both Williamson–Hall and Scherrer methods [14,15].

FTIR spectra of the as prepared samples, intermediates, and samples sintered at various temperatures, were recorded in KBr medium in the range 400–4000 cm^{-1} with a Thermo Nicolet Nexus FTIR (model 870).

TEM micrographs were obtained on a CM12 Phillips microscope operating at an accelerating voltage of 120 kV. The nanoparticles were dispersed in water by sonication and the TEM samples were prepared by placing a drop of the solution on a carbon-coated Cu grid and dried.

Laser Raman Microspectometry was done with a Renishaw Raman System 1000B coupled with a Leica DMLM microscope. The spectra were excited with 514 nm radiation from a 20 mW air cooled Argon ion laser and filtering of the Rayleigh scattering was achieved through an edge filter at 200 cm^{-1} cut off that allows study of Raman scattering only on the stokes side of the spectrum. Power at incidence on the sample surface was about 8 mW (at 100% laser power) with laser spot size of about 1.5 μm with 50× objective. Dispersion of the Raman scattering beam was achieved through prism and a 1800 L/mm grating with motorized movement. The system was calibrated with Ne lamp and accuracy of peak position was checked with Si standard. A Peltier cooled CCD detector of 578 × 400 pixels was used in which the image area was fixed within a window of 576 × 20 pixels. Spectra were acquired with the Windows Raman Environment (WiRE) software designed by the manufacturer that is integrated as a module to GRAMS (Galactic) for display of the spectral trace and various types of analysis of the spectrum. Acquisition of spectra was done in the extended scanning mode in the range 2000–200 cm^{-1} from the laser line. The laser power was controlled by use of neutral density (ND) filter and Raman scattering experiments were carried out at 1, 10, 25, 50 and 100% of the laser power.

3. Results and discussion

XRD pattern of the sample prepared in 1,4-butanediol shows that a spinel phase (O_h^7) is formed (Fig. 1). FTIR (Fig. 1 inset) also indicates the formation of a spinel phase. However, none of these results could identify the spinel phase, as γ-Fe_2O_3 or Fe_3O_4, as the lattice parameter values of both these ferrites are very close, i.e., 8.350 and 8.393 Å, respectively [16]. Moreover the lines in the XRD patterns of nanocrystalline materials are quite broad and accurate determination of lattice parameters to distinguish between γ-Fe_2O_3 and

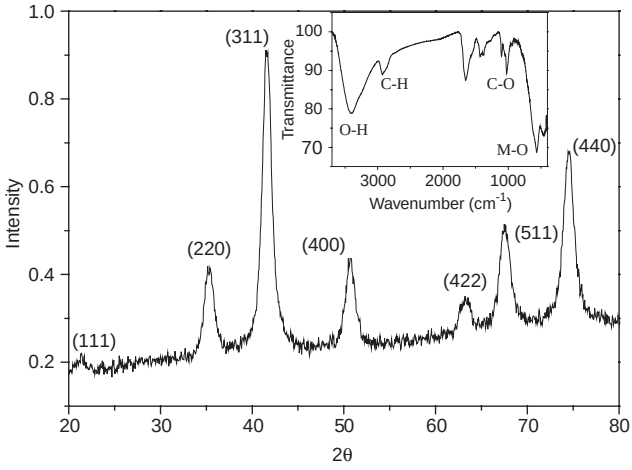

Fig. 1. X-ray diffraction pattern of 14BD sample and the inset shows the FTIR of the sample.

Fe_3O_4 is rather difficult. TEM micrograph (Fig. 2) shows that the sample is nanocrystalline without any agglomeration. Fig. 3a shows the Raman spectrum of the sample taken at low laser power (Lp) (10%). It shows broad bands at ~380, ~500, ~720, ~1450 and ~1580 cm^{-1} which are typical of γ-Fe_2O_3 as was found by de Faria et al. [17]. Thus it appears that the as prepared sample is γ-Fe_2O_3.

Most of the Raman studies on bulk iron oxides have been on Fe_3O_4 and α-Fe_2O_3. Fe_3O_4 has the spinel structure (O_h^7) with both Fe^{3+} and Fe^{2+} ions and gives rise to five Raman bands: three T_{2g}, one E_g and one A_{1g}. As reported in earlier studies only four bands at 193, 306, 538 and 668 cm^{-1} are observed [18]. α-Fe_2O_3 belongs to the D_{3d}^6 crystal space group and seven phonon lines are expected at 225, 247, 293, 299, 412, 498 and 613 cm^{-1}. In addition to these bands an intense band at 1320 cm^{-1} is observed due to a two magnon scattering which arises from the interaction of two magnons created on close antiparallel spin sites [19]. γ-Fe_2O_3 has an inverse spinel structure and can be seen as an iron deficient form of magnetite, with structural formula $Fe_{21.33}^{3+}\theta_{2.67}O_{32}^{2-}$, where $\theta_{2.67}$ means 2.67 vacancies in octahedral site of the spinel structure [20]. Raman spectrum of γ-Fe_2O_3 can be characterized by three broad bands around 350, 500 and 700 cm^{-1}, not present in the spectrum of any iron oxide or oxyhydroxide. However, in all the earlier reports additional broad bands at 1360 and 1580 cm^{-1} have also been observed [17,21]. Similar to Fe_3O_4, γ-Fe_2O_3 has the spinel structure but it also has considerable cation vacancies and the cations present are only Fe^{3+} ions. In the studies on CeO_{2-X} Spanier et al. [22] reported that the Raman spectra are likely to be directly affected by the presence of vacancies. Thus the broad bands found at 350, 500 and 700 cm^{-1} in γ-Fe_2O_3 could probably be due to the presence of vacancies in the spinel lattice. The band at 1360 cm^{-1} is very similar to that found in α-Fe_2O_3 which is antiferromagnetic and

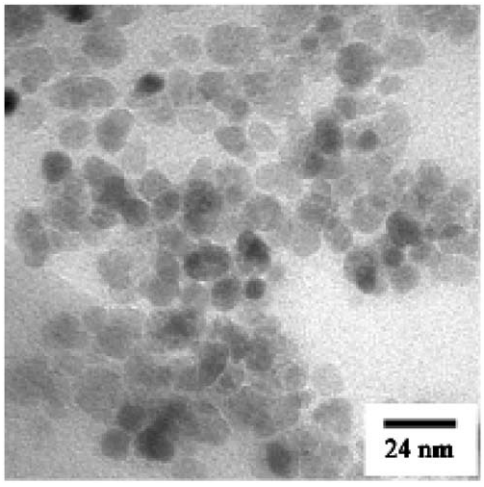

Fig. 2. TEM micrograph of the capped sample.

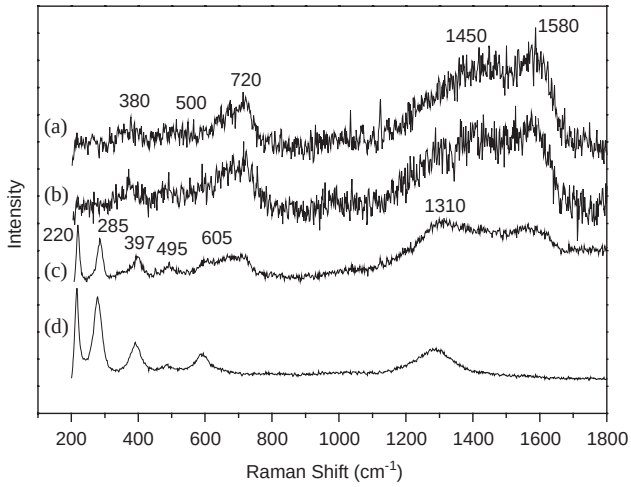

Fig. 3. Raman spectra of 14BD at (a) 10%, (b) 25%, (c) 50%, and (d) 100% Lp.

give rise to two magnon scattering arising out of the interaction of two magnons created on antiparallel close spin sites in the ferrite. Like all spinel ferrites γ-Fe_2O_3 is also ferrimagnetic, but the presence of cation vacancies in the octahedral site is not likely to allow a spin arrangement exactly similar to Fe_3O_4 and possibly the antiferromagnetic spin arrangement in this ferrite enables antiparallel close spin site similar to α-Fe_2O_3 and this may give rise to the observed band at 1320 cm^{-1}.

Figs. 3b–d show the spectra at various laser powers and Table 1 shows the phases present at various Lps. Table 1 shows that on increasing the Lp to 25%, the band positions remain unchanged implying that the γ-Fe_2O_3 sample is stable in Raman laser upto 25% Lp. On further increasing the laser power to 50%, however, Fig. 3c shows the presence of bands at 220, 285, 397, 495, 700, 1310 and 1580 cm^{-1}. Among these only ˜700 and 1580 cm^{-1} can be assigned to γ-Fe_2O_3 and the other five at 220, 285, 397, 495 and 1310 cm^{-1} are due to α-Fe_2O_3. Thus it appears that γ-Fe_2O_3 undergoes laser-induced degradation to α-Fe_2O_3. Similar laser induced degradation to α-Fe_2O_3 was earlier observed with bulk samples of Fe_3O_4 and various ferrihydrites [17,21]. However at 50% laser power γ-Fe_2O_3 is only partially degraded to α-Fe_2O_3 and a mixture of the two phases of iron oxide are shown in the Raman spectrum. But at 100% laser power complete degradation to α-Fe_2O_3 occurs as shown in Fig. 3d where six bands due to α-Fe_2O_3 at 218, 289, 392, 488, 590 and 1300 cm^{-1} are present. These band positions are slightly shifted to lower wave numbers from those found in Fig. 3c. Shifting of bands at higher Lp has been ascribed to local heating when the sample is subjected to higher laser power [17]. From these results it may be concluded that the γ-Fe_2O_3 sample prepared in 1,4-butanediol is stable upto 25% laser power, and then gradually degrades to α-Fe_2O_3 on increasing the Lp.

Table 1
Sample codes, sintering and refluxing temperatures, crystallite size and phases present

Sample	Sample code	Refuxing + sintering temp.	Lattice parameter (Å) + crystallite size (nm)	Laser power	Acquisition time (s)	Phase present
Diol capped γ-Fe_2O_3 prepared in 1,4-butanediol	14BD	483 K	8.36 + 9.5	10%	120	γ-Fe_2O_3
				25%	120	γ-Fe_2O_3
				50%	120	γ-Fe_2O_3 + α-Fe_2O_3
				100%	120	α-Fe_2O_3
γ-Fe_2O_3 prepared in 1,2-propanediol and sintered	12PD573	403 K + 573 K	8.36 + 10.2	10%	120	γ-Fe_2O_3
				25%	120	γ-Fe_2O_3
				25%	300	γ-Fe_2O_3 + α-Fe_2O_3
				50%	60	α-Fe_2O_3
	12PD673	403 K + 673 K	8.38 + 15.4	25%	120	γ-Fe_2O_3
				25%	300	γ-Fe_2O_3
				50%	120	α-Fe_2O_3
	12PD773	403 K + 773 K	8.38 + 48	1%	300	Fe_3O_4 + γ-Fe_2O_3
				10%	120	Fe_3O_4 + α-γ-Fe_2O_3
				25%	120	α-Fe_2O_3

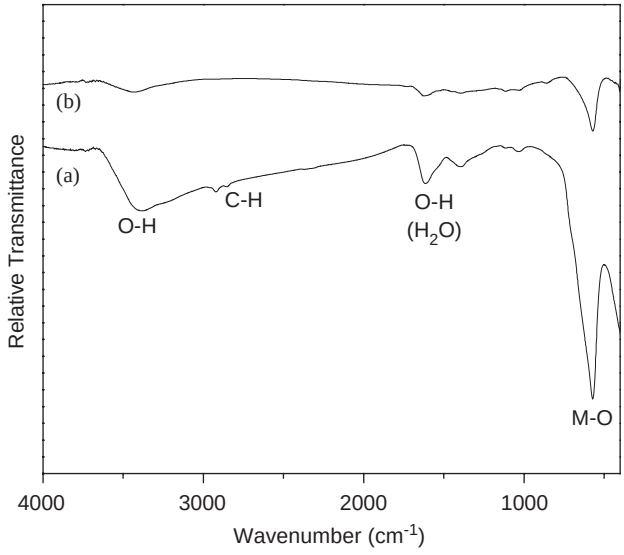

Fig. 4. FTIR spectra of 14BD sample heated at (a) 673 K and (b) 973 K.

Complete degradation is observed at 100% Lp. The γ-Fe_2O_3 sample prepared in 1,5-pentanediol also shows similar stability towards Raman laser. FTIR (Fig. 1 inset and Fig. 4) and dispersion studies on these samples have shown that the nanocrystalline γ-Fe_2O_3 prepared in 1,4-butanediol and 1,5-pentanediol are capped with the diol moiety and the capping is stable upto 873 K. Mössbauer studies also show the absence of any Fe^{3+} surface states which is expected as the organic moiety is present as capping on the surface [23]. Thus it appears that diol-capped γ-Fe_2O_3 is stable in Raman laser upto 25% laser power.

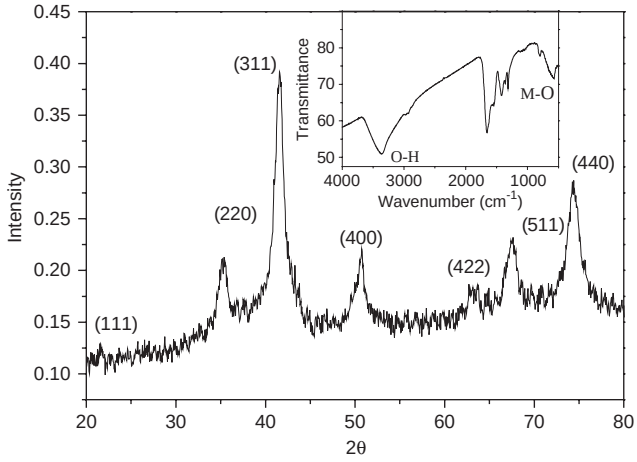

Fig. 5. X-ray diffraction pattern of 12PD573 sample and the inset shows the FTIR of the sample.

The samples prepared in 1,2-propanediol were sintered at 573, 673 and 773 K in argon atmosphere and the code names are given in Table 1. XRD of the 12PD573 sample (Fig. 5) shows the formation of the spinel phase and FTIR (Fig. 5 inset) shows the absence of any organic moiety in the sample, implying that nanocrystalline γ-Fe_2O_3 samples prepared in 1,2-propanediol however do not have the diol capping as is also evident from agglomeration of the nanocrystalline particles shown in TEM micrograph (Fig. 6). Thus it may be interesting to study its stability towards Raman Lp. The Raman spectrum of 1,2PD573 at 10% Lp with 120 s acquisition time (Fig. 7a) shows broad bands at ~390, ~500, ~710, ~1430 and 1580 cm^{-1}, characteristic of

γ-Fe_2O_3. On increasing the laser power to 25% (acquisition time 120 s), Fig. 7b shows that new bands at 219 and 276 cm^{-1} appear along with the bands of γ-Fe_2O_3. On increasing the acquisition time to 300 s, and keeping the laser power at 25%, Fig. 7c shows bands at 219, 276, 391, 590 and 1300 cm^{-1} due to α-Fe_2O_3 along with the band at 1580 cm^{-1}, due to γ-Fe_2O_3. Fig. 7d shows that at 50% Lp complete degradation of γ-Fe_2O_3 to α-Fe_2O_3 occurs. Thus it appears that in the uncapped sample, degradation of γ-Fe_2O_3 to α-Fe_2O_3 starts at lower Lp, i.e., 25%, whereas in case of 1,4-butanediol and 1,5-pentanediol capped γ-Fe_2O_3 samples, degradation starts at 50% laser power. These results clearly demonstrate for the first time that the stability of γ-Fe_2O_3 nanoparticles to Lp is increased by capping the sample. When the γ-Fe_2O_3 nanoparticles are capped there are no surface states (as shown by Mössbauer studies) and the sample is expected to be stable as it does not have the additional surface energy. In the uncapped samples, however surface states are present which causes these samples to be less stable. Thus not only does capping prevent agglomeration of the nanoparticles, it also improves dispersivity and stability of the samples.

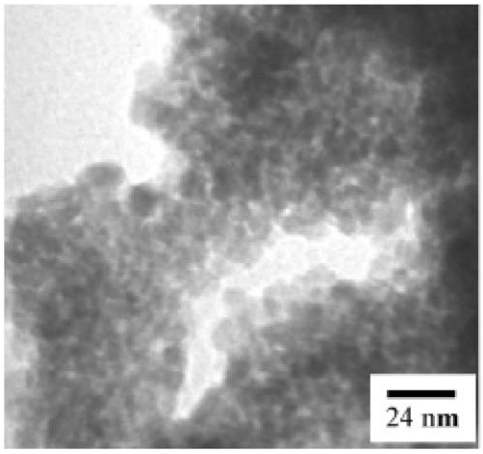

Fig. 6. TEM micrograph of uncapped sample.

The samples prepared in 1,2-propanediol were annealed in Ar atmosphere at different temperatures to vary the particle size (Table 1) and study the stability of these nanoparticles to Raman laser as a function of particle size. The Raman spectrum of 1,2PD673 sample (Fig. 8a) at 25% laser power and 120 s acquisition time shows broad bands at ~380, ~500, ~700, ~1390 and 1600 cm^{-1}, characteristic of γ-Fe_2O_3 similar to the spectrum of 1,2PD573 sample. On increasing the acquisition time to 300 s at 25% laser power (Fig. 3b) the spectrum remains unchanged indicating that under these conditions the sample remains as γ-Fe_2O_3. Thus by increasing the acquisition time to 300 s at 25% Lp, while 12PD573 sample (10.2 nm) degrades to α-Fe_2O_3 (Fig. 7c) 12PD673 sample (15.4 nm) remains stable (Fig. 8b). These results suggest that the stability of γ-Fe_2O_3 samples towards Raman laser increases with increasing crystallite size.

Both XRD and FTIR indicated that the 12PD773 sample has the spinel phase similar to the other samples. The Raman spectrum of this sample at 1% laser power and 300 s acquisition time, however shows the presence of bands at 300, 545 and 668 cm^{-1} (Fig. 9a). These bands are characteristic of Fe_3O_4 and not γ-Fe_2O_3. However, bands at 500 cm^{-1} and a shoulder at 710 cm^{-1} characteristic of γ-Fe_2O_3 are also present. These results suggest that the major phase present in the 1,2PD773 sample is Fe_3O_4 along with small amounts of γ-Fe_2O_3 phase. From XRD however, the presence of Fe_3O_4 and γ-Fe_2O_3 phases could not be ascertained. Formation of Fe_3O_4 along with some γ-Fe_2O_3 suggests that during heating the alkoxide at 773 K in argon atmosphere,

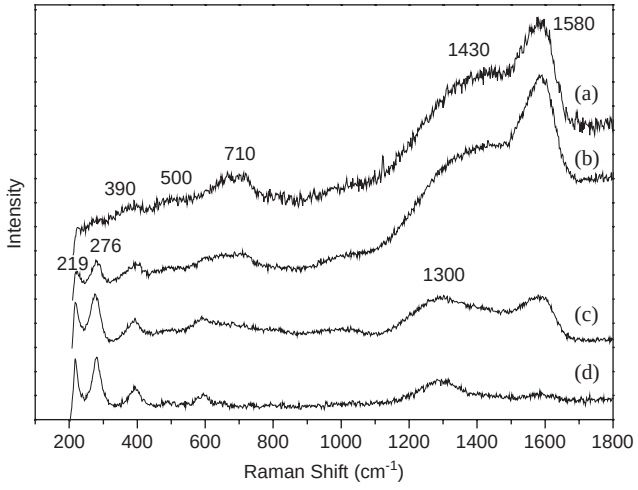

Fig. 7. Raman spectra of 12PD573 at (a) 10% Lp, (b) 25% Lp with 120 s acquisition time, (c) 25% Lp with 300 s acquisition time, and (d) at 50% Lp with 120 s acquisition time.

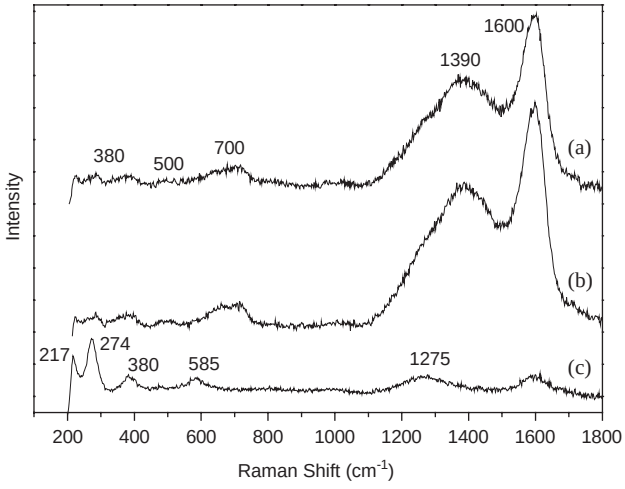

Fig. 8. Raman spectra of 12PD673 at (a) 25% Lp with 120 s acquisition time, (b) 25% Lp with 300 s acquisition time, and (c) at 50% Lp with 120 s acquisition time.

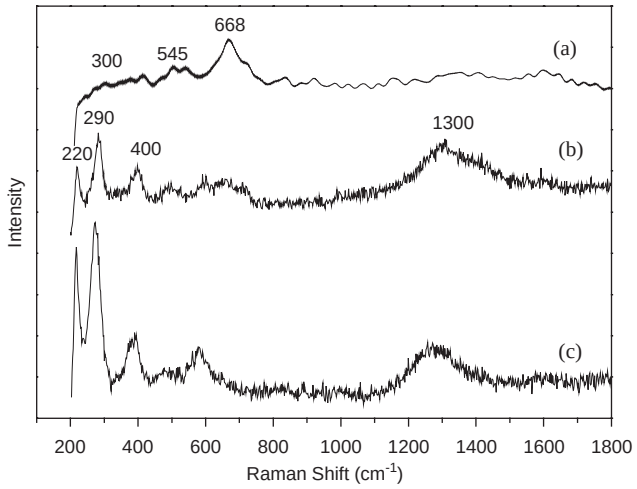

Fig. 9. Raman spectra of 12PD773 at (a) 1% Lp with 300 s acquisition time, (b) 10% Lp with 120 s acquisition time, and (c) at 25% Lp with 120 s acquisition time.

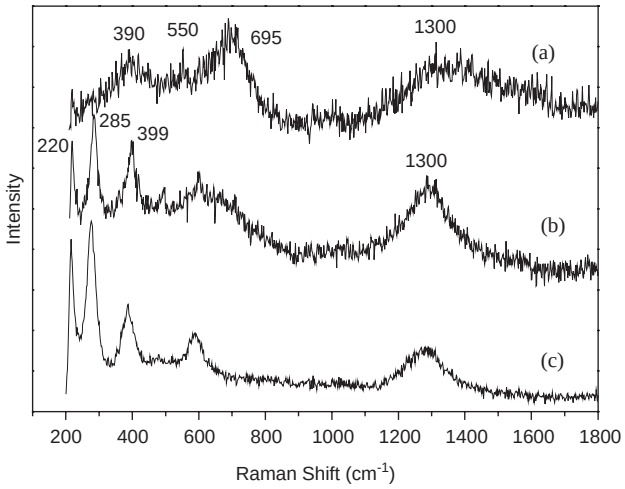

Fig. 10. Raman spectra of 6-line ferrihydrite prepared by the standard method at (a) 10% Lp, (b) 25% Lp, and (c) 50% Lp.

some of the Fe^{3+} ions are reduced to Fe^{2+} ions whereby Fe_3O_4 is formed. Reduction of Fe^{3+} was however not perceptible upto 673 K. The spectrum taken at 10% laser power shows bands of both Fe_3O_4 and α-Fe_2O_3 (Fig. 9b) implying that, nanocrystalline Fe_3O_4 degrades to α-Fe_2O_3 similar to bulk Fe_3O_4. Comparison of the results with γ-Fe_2O_3 shows that complete degradation of Fe_3O_4 occurs at a relatively lower laser power (Fig. 9c). From these results it may be concluded that γ-Fe_2O_3 nanoparticles are more stable to laser degradation than Fe_3O_4 nanoparticles.

During the synthesis of capped γ-Fe_2O_3 in 1,4-butanediol an intermediate was formed which was identified from XRD as 6-line ferrihydrite. A 6-line ferrihydrite was also prepared by the standard method and the stability of the two 6-line ferrihydrite samples were studied by Raman laser. The Raman spectra of 6-line ferrihydrite prepared by the standard method are shown in Fig. 10. The spectrum recorded at 10% laser power with 60 s acquisition time (Fig. 10a) shows broad weak bands at ~390, ~550 and ~1320 cm^{-1}, and a strong band at ~695 cm^{-1}. As reported by Mazzetti et al. [21] the presence of these bands are characteristic of 6-line ferrihydrite and the absence of the band in the region ~1580 cm^{-1} indicates the absence of any γ-Fe_2O_3. On increasing the laser power to 25%, Fig. 10b shows that new bands appear at 220, 285, 399 and 500 cm^{-1}, and the band at 1300 cm^{-1} becomes sharper. This appears to be due to the degradation of 6-line ferrihydrite to α-Fe_2O_3 although broadening of the band at 700 cm^{-1} implies that at this laser power only partial degradation occurs. On increasing the laser power to 50% however complete degradation to α-Fe_2O_3 is observed (Fig. 10c).

The Raman spectrum of the intermediate 6-line ferrihydrite is shown in Fig. 11a. The spectrum is

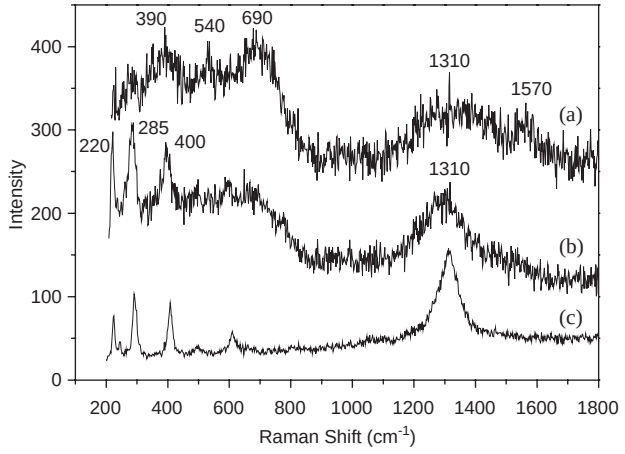

Fig. 11. Raman spectra of intermediate ferrihydrite at (a) 10% Lp (b) 25% Lp, and (c) 50% Lp.

similar to that of the 6-line ferrihydrite prepared by the standard method, with additional weak bands at ~1380 and ~1570 cm^{-1} due to γ-Fe_2O_3. This indicates that the intermediate formed is not just a 6-line ferrihydrite but has some γ-Fe_2O_3 phase in it. This implies that during refluxing, γ-Fe_2O_3 phase is formed much below 483 K and can be detected in the intermediate isolated at 413 K by Raman spectroscopy. The presence of small amounts of γ-Fe_2O_3 in the intermediate ferrihydrite could not be detected in the XRD analysis because of the identical position of the most intense peak of γ-Fe_2O_3 (311) and 6-line ferrihydrite (110). On increasing the laser power to 25% (Fig. 11b) and then to 50% (Fig. 11c) the intermediate is completely degraded to α-Fe_2O_3. These results imply that the stability towards Lp is same for the intermediate and the standard 6-line ferrihydrite sample.

4. Conclusion

From the results it may be concluded that Raman spectroscopy is a useful technique to identify the spinel phase of iron oxide. Thus, that the spinel phase formed by refluxing ferric nitrate in diol is γ-Fe_2O_3 and not Fe_3O_4 could not be ascertained by XRD but could be identified from its Raman spectra. The results also show that capping of the γ-Fe_2O_3 nanoparticles makes it more stable towards Raman laser degradation. Increasing the particle size also increases the stability. However, Fe_3O_4 with a larger particle size, i.e., 48 nm is less stable than γ-Fe_2O_3 even when it has a smaller particle size, i.e., 10.2 nm.

References

[1] T.A. Sorenson, S.A. Morton, G.D. Waddill, J.A. Switzer, J. Am. Chem. Soc. 124 (2002) 7608.
[2] T. Nakamura, T. Miyamoto, Y. Yamada, J. Magn. Magn. Mater. 256 (2003) 340.
[3] C.C. Berry, A.S.G. Curtis, J. Phys. D:: Appl. Phys 36 (2003) R198.
[4] D.E. Speliotis, J. Magn. Magn. Mater. 193 (1999) 29.
[5] R.M. Cornell, U. Schwertmann, The Iron Oxides, VCH, Weinheim, Germany, 1996, p. 463.
[6] S.P. Bhatnagar, R.E. Rosensweig, J. Magn. Magn. Mater. 149 (1995) 198.
[7] V.E. Fertman, Magnetic Fluid Guide Books: Properties and Applications, Hemisphere Publishing Co., New York, 1990.
[8] J. Moser, S. Punchihewa, P.P. Infelta, M. Grätzel, Langmuir 7 (1991) 3012.
[9] P. Hermetin, R. Doenges, V. Franssen, C. Bieva, F.J.V. Brugghen, Bioconjugate Chem. 1 (1990) 411.
[10] A. Kuznetsov, V.I. Filippov, O.A. Kuznetsov, V.G. Gerlivanov, E.K. Dobrinsky, S.I. Malashin, J. Magn. Magn. Mater. 194 (1999) 22.
[11] P.C. Morais, S.W. da Silva, M.A.G. Soler, N. Buske, J. Phys. Chem. A 104 (2000) 2894.
[12] S.W. da Silva, M.A.G. Soler, C. Gansau, N. Buske, P.C. Morais, J. Magn. Magn. Mater. 226–230 (2001) 1890.
[13] O.N. Shebanova, P. Lazor, J. Raman Spectrosc. 34 (2003) 845.
[14] G.K. Williamson, W.H. Hall, Acta. Metall. 1 (1953) 22.
[15] B.D. Cullity, Elements of X-ray Diffraction, Reading, MA, Addison-Wesley Publishing Company, INC., 1978, p. 102.
[16] JCPDS Code No: (a) [24-0081] and (b) [85-1436].
[17] D.L.A. de Faria, S.V. Silva, M.T. de Oliveira, J. Raman Spectrosc. 28 (1997) 873.
[18] O.N. Shebanova, P. Lazor, J. Solid State Chem. 174 (2003) 424.
[19] T.R. Hart, S.B. Adams, H. Tempkin, in: M. Balkanski, R. Leite, S. Porto (Eds.), Proceedings of the Third International Conference on Light Scattering in Solids, Flammarion, Paris, 1976, p. 259.
[20] G.A. Ferguson, M. Hass, Phys. Rev. 112 (1958) 1130.
[21] L. Mazzetti, P.J. Thistlethwaite, J. Raman Spectrosc. 33 (2002) 104.
[22] J.E. Spanier, R.D. Robinson, F. Zhang, S.W. Chan, I.P. Herman, Phys. Rev. B 64 (2001) 245407.
[23] J. Ghose, K.S.K. Varadwaj, D. Das, Hyperfine Interactions, in press.